



PCCP

Three-Dimensional Auxetic Properties in Group V-VI Binary Monolayer Crystals X_3M_2 ($X=S, Se$; $M=N, P, As$)

Journal:	<i>Physical Chemistry Chemical Physics</i>
Manuscript ID	CP-ART-08-2018-005260.R1
Article Type:	Paper
Date Submitted by the Author:	08-Nov-2018
Complete List of Authors:	Chen, Yan; Xi'an Jiaotong University, School of Aerospace Liao, Xiangbiao; Columbia University, Earth and Environmental Engineering Shi, Xiaoyang; Columbia University, Earth and Environmental Engineering Xiao, Hang; Columbia University, Liu, Yilun; Xi'an Jiaotong University, School of Aerospace Chen, Xi; Columbia University

SCHOLARONE™
Manuscripts

Three-Dimensional Auxetic Properties in Group V-VI Binary Monolayer Crystals X_3M_2 ($X=S, Se$; $M=N, P, As$)

Yan Chen¹, Xiangbiao Liao⁴, Xiaoyang Shi⁴, Hang Xiao^{2,4,*}, Yilun Liu^{3,*} and Xi Chen^{2,4}

¹ International Center for Applied Mechanics, State Key Laboratory for Strength and Vibration of Mechanical Structures, School of Aerospace, Xi'an Jiaotong University, Xi'an 710049, China

² School of Chemical Engineering, Northwest University, Xi'an 710069, China

³ State Key Laboratory for Strength and Vibration of Mechanical Structures, School of Aerospace, Xi'an Jiaotong University, Xi'an 710049, China

⁴ Center for Advanced Materials for Energy and Environment, Department of Earth and Environmental Engineering, Columbia University, New York, NY 10027, USA

* E-mail: (Y.L.) yilunliu@mail.xjtu.edu.cn; (H.X.) hx2152@columbia.edu

Abstract: The mechanical behaviors for a series of two-dimensional (2-D) crystals X_3M_2 ($X=S, Se$; $M=N, P, As$) are explored through density functional theory (DFT) calculations. Two atomic structures exist for 2-D X_3M_2 , namely α -heart and β -heart, which exhibit different out-of-plane Negative Poisson's Ratio (NPR) phenomena. For α -heart structure, general out-of-plane NPR exists under in-plane tension in y direction, while for β -heart type structures general NPR exists under in-plane tension in x direction. Through DFT calculations, we revealed that NPR is a general phenomenon for 2-D X_3M_2 with heart-shaped atomic structures, and the absolute value of out-of-plane NPR for 2-D X_3M_2 is always one order of magnitude larger than other 2-D crystals reported before. At the same time, in-plane NPR at certain angles around two in-plane principal axes also exists for 2-D X_3M_2 except S_3P_2 due to the special heart-shaped structure. Coexistence of out-of-plane and in-plane NPR for 2-D crystals has not been reported before and these special three-dimensional (3-D) auxetic properties in 2-D crystals may enormously enrich the researches on novel mechanical, electrical and chemical behaviors of 2-D crystals. This discovery will extend the family of 2-D crystals with NPR, and also provided new insights for designing novel negative Poisson's ratio materials.

1. Introduction

The success of graphene¹ has inspired great efforts to discover other two-dimensional (2-D) materials with excellent mechanical, electrical and chemical performances. Today, 2-D materials beyond graphene have covered more and more elements in the periodic table.²⁻⁸ More and more mono-element 2-D materials have been discovered by density functional theory (DFT) calculations or experiments. For example, 2-D borophene (group-III element) has been successfully prepared on silver surfaces with metallic characteristics.⁹ For group-IV elements, silicene, germanene, stanine have been all successfully synthesized in experiment besides graphene.¹⁰⁻¹³ For group-V elements, all of the phosphorus, arsenic, antimony and bismuth have stable monolayer sheets (i.e. arsenene, antimonene, and bismuthene).^{7, 14-16} Of course, the family of 2-D materials composed of more than one chemical element is huge, such as monolayer materials of group V-VI elements,¹⁷ transitional metal dichalcogenides (TMDs),¹⁸ MXenes,¹⁹ etc. In most cases, some similar features are observed for 2-D materials with the same groups in element periodic table, such as atomic topological structure, energy band structure, electronic properties, etc.^{7, 17, 20}

Poisson's ratio is one of the basic material parameters, defined as the negative value of the lateral strain to applied strain. Normally, Poisson's ratio is positive for most materials. Intriguingly, negative Poisson's ratio (NPR) materials, also known as auxetic materials, attracts considerable research interest, since the foam structure with NPR have been proposed by Lakes in 1987.²¹ Then, a few natural materials such as cubic metals²² and zeolites²³ were also found to be the auxetic materials. Very recently, lots of artificial structures are designed to be auxetic materials, such as designable compliant micromechanisms,²⁴ metal-organic frameworks,²⁵ soft metamaterials,²⁶ origami structures,²⁷ protein crystals.²⁸ Special re-entrant architectures and chiral honeycomb structures are the main causes of auxetic phenomenon.^{21, 29, 30} The auxetic structures usually enhance some the mechanical properties of the auxetic materials, including shear moduli, indentation resistance, tear resistance and fracture toughness,³¹⁻³³ expected to be applied to a wide range of fields, such as drug release, bioengineering, textiles, fasteners,³⁴⁻³⁶ and greatly enriching the material design methods and their functionality.

Inspired by substantial researches on auxetic effect of three-dimensional (3-D) or bulk materials, a number of 2-D crystals have been found to exhibit intrinsic auxetic behaviors. Due

to the structural uniqueness of 2-D crystals, out-of-plane NPR and in-plane NPR are found in succession for some nonplanar 2-D crystals. Here, the out-of-plane strain is defined as the thickness change ratio between the outmost atoms of the nonplanar 2-D crystals. For instance, black phosphorene-like structures³⁷, including monolayer BP₅,³⁸ arsenene³⁹ and SnSe⁴⁰ have been predicted to have a small intrinsic out-of-plane NPR by DFT calculations due to their unique puckered structure, of which out-of-plane NPR for black phosphorene have already been observed in experiment by Du. et al.⁴¹ What's more, borophane (hydrogenated borophene) were predicted to have out-of-plane NPR under armchair tension as well.⁴² Besides, many carefully designed 2-D crystals are predicted to have intrinsic in-plane NPR, such as penta-graphene,⁴³ Be₅C₂,⁴⁴ δ -phosphorene,⁴⁵ siligraphene SiC₆.⁴⁶ However, the previously discovered intrinsic NPR of 2-D crystals focuses on the 2-D materials with puckered structure. As the continuous increasing of 2-D material family with different atomic structures, the relation between the intrinsic NPR of 2-D crystals and their atomic structures is far from well-studied. Besides, different from the artificial structures whose mechanical properties can be predicted by the continuum deformation of their structural ligaments, the quantum and non-local effects may lead completely different mechanical behaviors for 2-D crystals with the same atomic structures. Therefore, the achievements in artificial structures cannot be directly applied to the 2-D crystals.

In this study, we focus on studying the mechanical behaviors of monolayer structures of group V-VI elements with special heart-shaped structure, i.e. X₃M₂ (X=S, Se; M=N, P, As). Recently, two novel 2-D crystals S₃N₂ and S₃P₂ have been predicted through DFT calculations by Hang et al.,^{47, 48} before which the crystal structures (in bulk form) of S₃As₂ and Se₃As₂ are found to be layered heart-shaped structures in experiment.^{49, 50} These 2-D crystals with intriguing heart-shaped structures remain many mysteries to be explored, such as their unusual mechanical properties. Through DFT calculations, we revealed that NPR is a general phenomenon for all 2-D X₃M₂ (X=S, Se; M=N, P, As), and two new structures (i.e. α -heart and β -heart) are proposed to cause NPR. Furthermore, out-of-plane NPR and in-plane NPR may coexist due to their special atomic structures. For the first time, we revealed that 3-D auxetic properties may exist in the family of 2-D crystals. Our results may extend the family of 2-D crystals with NPR, and also provided new insights for designing materials with novel mechanical properties, such as large negative Poisson's ratio in three orthogonal directions.

2. Models and Methods

Three elements of group-V and two elements of group-VI are considered in this study (see inset of Figure 1) for group V-VI binary monolayer crystals X_3M_2 ($X=S, Se$; $M=N, P, As$). The minimum-energy structures for 2-D X_3M_2 have two different atomic structures, i.e. α -heart and β -heart, as shown in Figure 1. Although the top view of S_3N_2 and S_3P_2 ^{47, 48}(see Figure S1 for other atomic structures of 2-D X_3M_2 in detail) are similar, their relative position of atoms X and M is different, which can be clearly observed in the front and side views in Figure 1. Such subtle differences of the atomic structure will lead to completely different Poisson's ratio in the out-of-plane direction under in-plane tension.

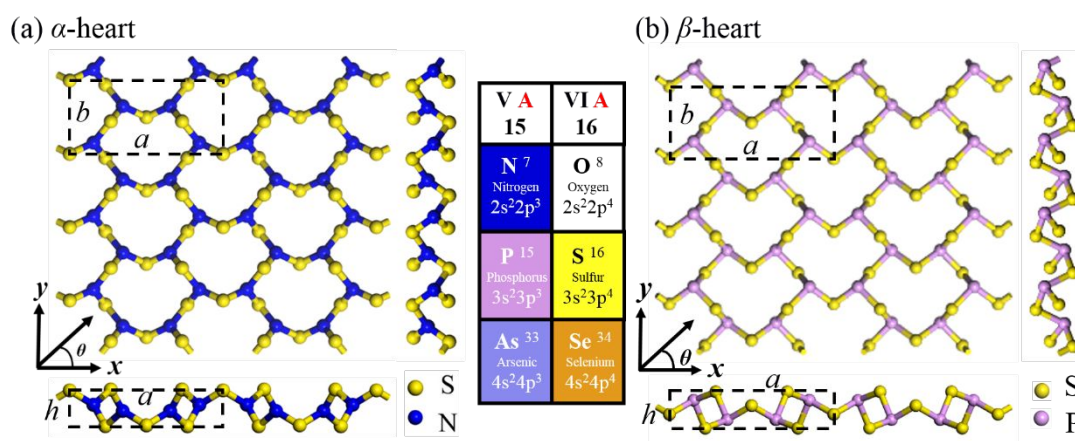


Figure 1 Atomic structures for two 2-D crystal X_3M_2 . (a) α -heart, S_3N_2 and (b) β -heart, S_3P_2 . The inset shows group-V and VI elements considered in this study (colored). θ defines the orientation relative to x axis.

All *ab initio* DFT calculations were performed using QUANTUM ESPRESSO.⁵¹ The generalized gradient approximation (GGA) with Perdew, Burke, and Ernzerhof (PBE) parametrization was adopted for the exchange-correlation functional.⁵² The electron-ion interaction was described by ultrasoft pseudopotentials, a plane-wave cutoff energy of 50 Ry for electron wavefunctions was used, and brillouin zone for the supercells was sampled by a $5 \times 11 \times 1$ Monkhorst-Pack k -point mesh.⁵³ The system convergence was tested for cutoff energy and k -point mesh. A vacuum layer of 16 Å was introduced in the perpendicular direction of the basal plane to minimize the interlayer interactions due to the periodic boundary condition. All

the structures were first relaxed without any symmetry constraint using conjugate gradient method (CG) until the energy and Hellmann-Feynman force were converged within 10^{-7} eV and 10^{-3} eVÅ⁻¹, respectively. The relaxed lattice constants for 2-D X₃M₂ (X=S, Se; M=N, P, As) are summarized in Table 1.

The true thickness h of 2-D X₃M₂ was defined as the coordinate difference of the outmost X and M atoms in z direction. To get the effective thickness d of 2-D X₃M₂ (for calculation of Young's modulus), a van der Waals (vdW) correction proposed by Grimme (DFT-D2)⁵⁴ was chosen to optimize the bulk crystal structures of layered X₃M₂ (X=S, Se; M=N, P, As). The cohesive energy is defined as,

$$E_c = \frac{3E(X) + 2E(M) - E(X_3M_2)}{5}$$

where $E(X_3M_2)$ stands for energy of 2-D X₃M₂ after optimization, $E(X)$ and $E(M)$ are the energy of single atom X or M, respectively.

3. Results and Discussions

The basic parameters of 2-D X₃M₂ after energy minimization are shown in Table 1. For the same atomic structural type, the true thickness h and effective thickness d will increase with the atomic number of X or M, note that the in-plane area of 2-D X₃M₂ also follows the same trend. The energy band structures are also calculated (see Figure S2), which are mainly determined by atomic structure of 2-D X₃M₂, i.e. α -heart atomic structure corresponds to direct energy band structure while β -heart atomic structure exhibits in-direct energy band structure. The band gap E_g for 2-D X₃M₂ are shown in Table 1, and we can conclude that for the same atomic structure, the band gap E_g decreases with increasing the atomic number of X or M. Note that, band gaps will be underestimated by the GGA level DFT calculations^{55,56}, our purpose will be focused on the trend the gap follows.

Table1 Calculated basic parameters for 2-D X₃M₂ (M=N, P, As, X=S, Se)

Type	Formula	a (Å)	b (Å)	h (Å)	d (Å)	E_g (eV)	E_c (eV/atom)
α	S ₃ N ₂	8.861	4.254	2.099	5.079	2.015	3.339
	Se ₃ N ₂	9.735	4.338	2.374	5.144	1.420	2.958
β	S ₃ P ₂	10.714	4.704	2.405	4.687	2.509	3.508

Se ₃ P ₂	11.410	4.747	2.672	5.018	2.027	3.158
S ₃ As ₂	11.340	4.632	2.579	4.866	2.306	3.304
Se ₃ As ₂	12.075	4.535	2.895	4.882	1.766	3.039

3.1 Significant negative Poisson's effect in out-of-plane direction

Out-of-plane NPR is an interesting phenomenon found in a few 2-D crystals, such as black phosphorene, Arsenene, monolayer BP₅ and Tinselenidene³⁷⁻⁴⁰, which means the thickness of these 2-D crystals increases under in-plane tension. As we know, except hydrogenated borophene (i.e. borophane usually exhibiting some wrinkles⁴²), other 2-D crystals with out-of-plane NPR have similar topological structures as that of black phosphorene, i.e. the puckered structure.³⁷⁻⁴⁰ The question is, whether the puckered structure is the unique structure for out-of-plane NPR of 2-D crystals and there are some 2-D crystals with unusual NPR in both of the in-plane and out-of-plane directions?

For α -heart structure S₃N₂, Figure 2(a) illustrates the out-of-plane strain under uniaxial tension in x direction. When the applied strain ε_x is smaller than 0.185, the out-of-plane strain ε_H first increases to the maximum value of about 0.025, and then decreases to about 0.009 at $\varepsilon_x = 0.185$, after which a small increasing of ε_x leads abrupt drop of ε_H to a negative value caused by the structural transition of S₃N₂ that is the red circle marked region will rotate a certain angle to get a minimum energy state, as shown in the inset of Figure 2(a). The similar structural transition of Se₃N₂ is also observed, but positive Poisson's ratio is obtained due to different motion of X and M atom in Se₃N₂ during in-plane tension which will be further analyzed in the following content, as shown in Figure S3.

The out-of-plane Poisson's ratio is defined as the negative value of the out-of-plane strain to the in-plane applied strain, i.e. $\nu_{iH} = -\frac{\varepsilon_H}{\varepsilon_i}$, $i = x, y$. Figure 2(b) shows the ν_{xH} under different in-plane applied strain ε_x . The out-of-plane Poisson's ratio is negative till the structural transition at $\varepsilon_x = 0.185$ with a minimum value of -0.695 at $\varepsilon_x = 0.010$. Here, the structural transition causes the abrupt change of the Poisson's ratio, which also holds for other 2-D X₃M₂ with structural transition as shown below. Figure 2(c) shows the structural transition of S₃N₂ at strain $\varepsilon_x = 0.120$ with respect to its equilibrium configuration. The small increase of thickness of S₃N₂ can be observed with the help of the blue dashed line.

When uniaxial tension is applied in y direction, an interesting demarcation point is

observed, where the out-of-plane strain ε_H gets the minimum value of -0.0177 at $\varepsilon_y = 0.030$. After that, the strain ε_H continuously increases to become positive. The demarcation point is caused by the abrupt change of the outmost atoms of S_3N_2 during in-plane tension which is used to define its thickness, as shown in the inset of Figure 2(d). Indeed, this type of structural transition is a general phenomenon for all of the 2-D crystals X_3M_2 , which will be explained in detail below. Figure 2(e) shows the out-of-plane Poisson's ratio ν_{yH} under uniaxial tension in y direction. The out-of-plane Poisson's ratio ν_{yH} changes from positive value to negative value at about $\varepsilon_y = 0.042$ due to the change of outmost atoms and it gets a minimum value of -0.754 at $\varepsilon_y = 0.120$. Figure 2(f) shows the obvious increase of the thickness of S_3N_2 at strain $\varepsilon_y = 0.280$ with respect to the equilibrium configuration.

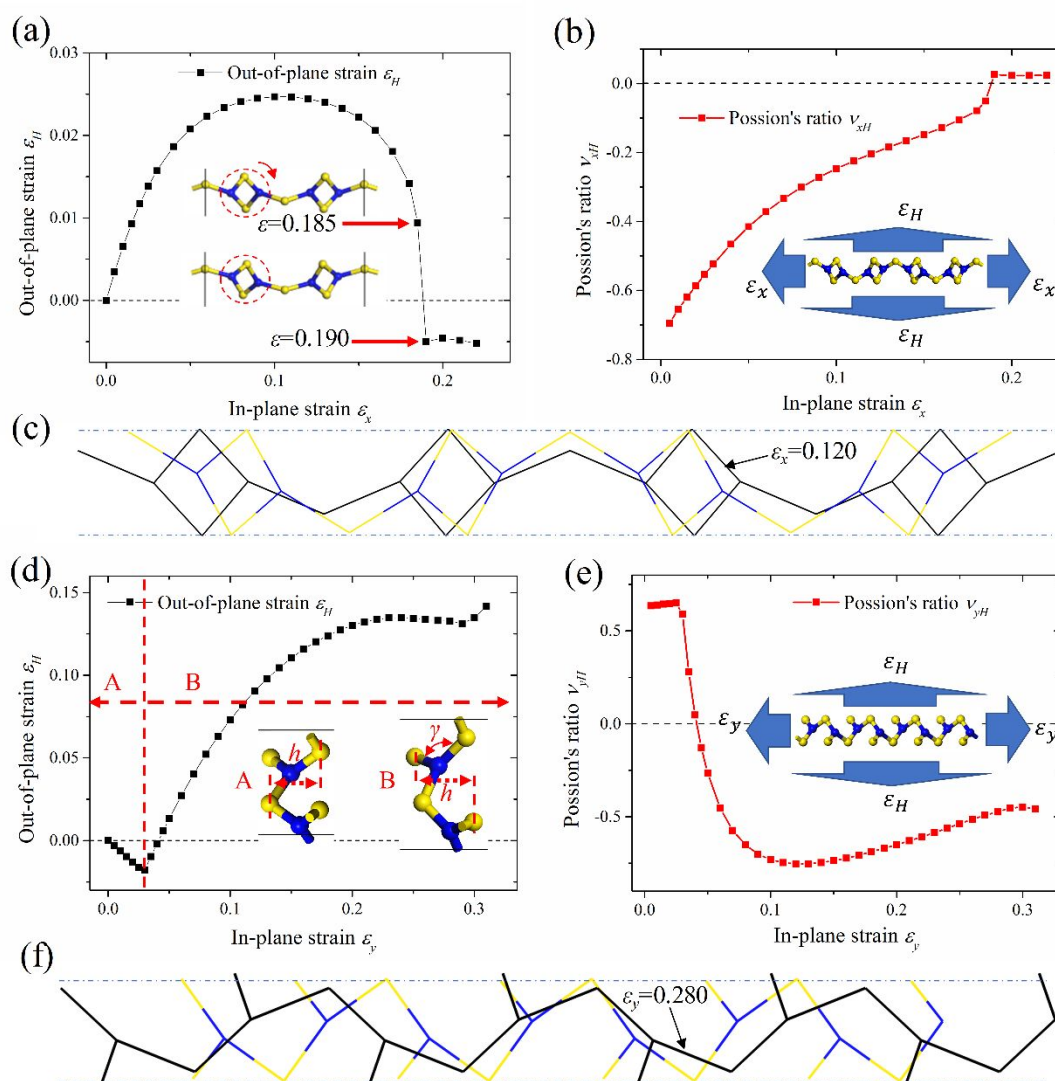


Figure 2. Out-of-plane deformation of α -heart structure S_3N_2 under in-plane tension. Out-of-plane strain (a) and the corresponding Poisson's ratio (b) under uniaxial tension in x direction ε_x . Out-of-

plane strain (d) and the corresponding Poisson's ratio (e) under uniaxial tension in y direction. The thickness change of monolayer S_3N_2 at $\varepsilon_x = 0.120$ (c) and $\varepsilon_y = 0.280$ (f), respectively. The blue dashed lines in (c) and (f) indicate the thickness of the equilibrium structure of S_3N_2 . Black color represents the deformed configuration and the colored configuration represents the equilibrium structure.

While for β -heart structures, taking S_3P_2 as an example (see Figure S4-S6 for the results of S_3As_2 , Se_3As_2 and Se_3P_2), the results are different. Figure 3 illustrates the out-of-plane deformation of S_3P_2 under in-plane tension. When uniaxial tension is applied in x direction, the out-of-plane strain ε_H is always positive as ε_x increases till the failure of S_3P_2 (see figure 3(a)), although it shows a sinusoidal shape. Correspondingly, Figure 3(b) gives the out-of-plane Poisson's ratio ν_{xH} of S_3P_2 which is negative till the failure of S_3P_2 . Here, the Poisson's ratio of S_3P_2 first quickly increases with the applied strain ε_x for $\varepsilon_x < 0.11$, and then its change is small. Figure 3(c) shows the atomic structure of S_3P_2 at $\varepsilon_x = 0.110$ compared to that of the equilibrium configuration, and a small increase of the thickness is observed. When uniaxial tension is applied in y direction, the demarcation point is also observed due to the change of outmost atoms, similar to S_3N_2 except that it occurs at a much larger strain (see Figure 3(d)). Thus, although the out-of-plane Poisson's ratio quickly decreases after the demarcation point, it is still positive till the failure of S_3P_2 .

The comparison of the out-of-plane Poisson's ratio for 2-D X_3M_2 ($X=S, Se; M=N, P, As$) and other 2-D crystals reported before is presented in Table 2. Here, the absolute value of out-of-plane NPR of 2-D X_3M_2 ($X=S, Se; M=N, P, As$) is much larger than that of other 2-D crystals reported before, i.e. the largest absolute value of out-of-plane NPR reported before is 0.171 for Tinselenidene ($SnSe$)⁴⁰ and others are all below 0.1, while for 2-D crystals X_3M_2 the minimum is 0.556 for Se_3As_2 and the maximum is 1.292 for S_3As_2 . In general, it is an order of magnitude larger (see Table 2). For bulk X_3M_2 crystals formed by stacking their 2-D crystal counterpoints, the most energetically favorable stacked bulk crystals are also different for α -heart and β -heart X_3M_2 (see Figure S8). It is interesting that all the α -heart X_3M_2 bulk crystals exhibit positive cross-plane interlayer Poisson's ratio under both in-plane tensions (x or y), as shown in Figure S9 and S10. While cross-plane interlayer NPR can be observed under tension in the y direction

for all the β -heart X_3M_2 bulk crystals, although the corresponding absolute values are much smaller than their 2-D crystal counterparts (see Figure S11~S14). The comparison of cross-plane interlayer Poisson's ratio for X_3M_2 bulk crystals ($X=S, Se; M=N, P, As$) and other reported bulk crystals (see Table S1) shows that the absolute values of cross-plane interlayer NPR of S_3P_2 and Se_3P_2 bulk crystals are comparative with black phosphorus⁴¹ and bulk arsenene³⁹, thus can be verified by analyzing the evolution of the Raman spectra, as demonstrated in the study of bulk black phosphorus⁴¹.

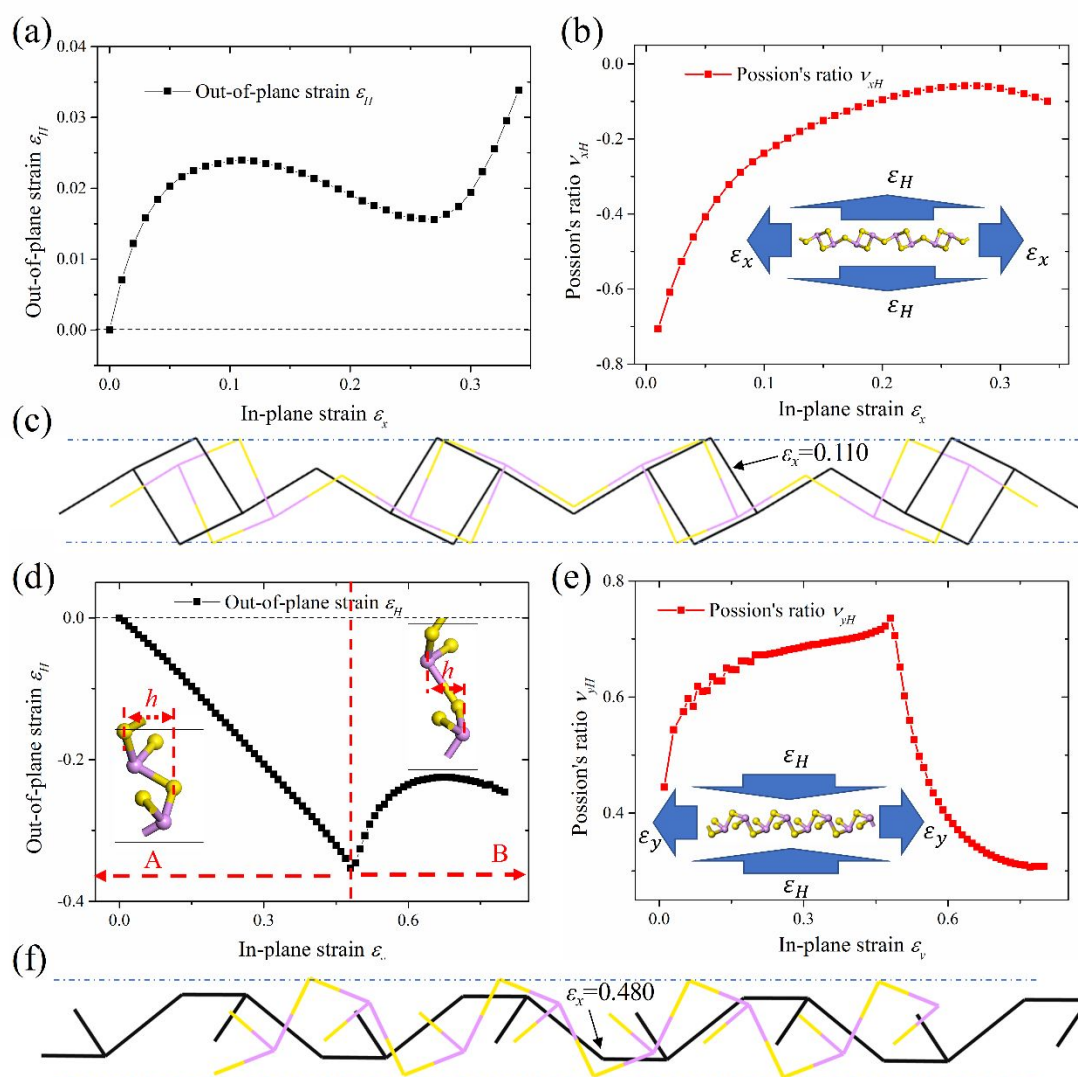


Figure 3. Out-of-plane deformation of β -heart structure S_3P_2 under in-plane tension. Out-of-plane strain (a) and the corresponding Poisson's ratio (b) under uniaxial tension in x direction. Out-of-plane strain (d) and the corresponding Poisson's ratio (e) under uniaxial tension in y direction. The thickness change of monolayer S_3P_2 at $\epsilon_x = 0.110$ (c) and $\epsilon_y = 0.480$ (f), respectively. Black color represents the deformed configuration and the colored configuration represented the equilibrium configuration.

What's more, the out-of-plane NPR for S_3N_2 coexists for uniaxial tension in both of the x and y direction, which is the first reported for 2-D crystals as we know. Normally, out-of-plane NPR only exists in uniaxial tension of one direction, even for other 2-D crystals X_3M_2 ($X=S, Se$; $M=N, P, As$) except S_3N_2 . Thus, the question is why the novel heart-shaped topological structures can lead to the general out-of-plane NPR for α -heart and β -heart structures under tension in the y and x direction, respectively. The underlying mechanism will be presented below.

Table 2 Out-of-plane Poisson's ratio for X_3M_2 ($X=S, Se$; $M=N, P, As$) and other 2-D crystals reported before.

	ν_{xH}	ν_{yH}
Black phosphorene ³⁷	0.046	-0.027
BP ₅ monolayer ³⁸	/	-0.037
Tinselenidene (SnSe) ⁴⁰	-0.171	0.460
Arsenene ³⁹	0.130	-0.093
Borophane ⁴²	-0.053	0.160
S_3N_2	-0.695	0.634 (-0.754)*
Se_3N_2	0.164	0.399 (-0.288)*
S_3P_2	-0.706	0.444
Se_3P_2	-0.679	0.637
S_3As_2	-1.292	0.293
Se_3As_2	-0.556	0.575

* The brackets here mean that the Poisson's ratio changes sign during in-plane tension. The value before brackets is the Poisson's ratio at in-plane strain 0.01, i.e. near the equilibrium configuration, and the value in brackets is the smallest Poisson's ratio.

Figure 4 indicates the motion of different atoms of 2-D X_3M_2 during in-plane tension. For α -heart structure S_3N_2 under uniaxial tension in y direction, the dihedral angle φ_1 decreases

and dihedral angle φ_2 increases, which has a lifting effect on atom S1, as shown in Figure 4(a) and 4(a). As a result, the z position of atom S1 increases and the z position of atom S2 decreases with increasing ε_y . Initially, the z position of atom S1 is lower than that of atom S2, and the thickness defined with atom S2 decreases as atom S2 moves down, which leads to the initial positive Poisson's ratio. After the height of atom S1 exceeds that of atom S2, atom S1 becomes the outmost atom and the thickness is defined with atom S1, leading to the out-of-plane NPR, just as shown in the inset of Figure 2(d). The intersect point of the height between atom S1 and atom S2 corresponds to the demarcation point shown in Figure 2(d). Note that, bond length S1-N1 changes little with increasing ε_y (see Figure S7). Thus, the out-of-plane NPR of α -heart structures is mainly attributed to the change of dihedral angle during in-plane tension.

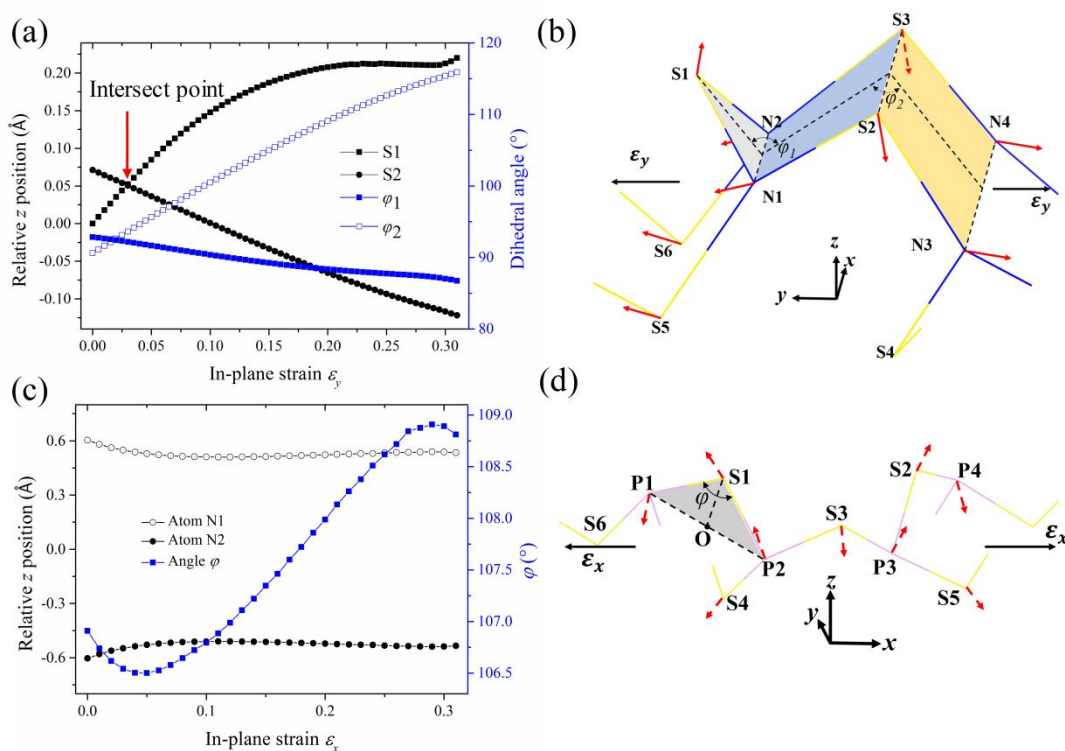


Figure 4. Mechanism of general out-of-plane NPR for α -heart and β -heart structures. (a) Relative position of atom S1 and S2 in z direction to the initial position of atom S1 and dihedral angle φ_1 and φ_2 for S_3N_2 with respect to ε_y and (b) schematic diagram for atom motion for S_3N_2 under uniaxial tension in y direction. (c) Relative position in z direction of atom P1 and P2 and angle φ for S_3P_2 with respect to ε_x and (d) schematic diagram for atom motion for S_3P_2 under uniaxial tension in x direction.

For β -heart structure S_3P_2 under uniaxial tension in x direction, atom P1 moves downward

and atom P2 moves upward, and the triangle S1-P1-P2 turns anticlockwise, as shown in Figure 4(d). The point O (Figure 4(d)) remains fixed due to structural symmetry of S_3P_2 under uniaxial tension in x direction. On the other hand, both of the bond length S1-P1 and S1-P2 increase with ε_x (see Figure S7). Consequently, the atom S1 moves upward quickly as angle φ decreases, which causes quick increase of the out-of-plane strain in the beginning and end tension of Figure 4(a). While, the lifting effect by the increase of angle φ at the middle part is canceled by the bond length increase and counter clockwise rotation of OS1, which causes a small drop of ε_H (see Figure 4(a)). In summary, the increase of bond length and the rotation of local structure attribute to the out-of-plane NPR of β -heart structures under tension in the x direction, different from α -heart structures.

3.2 Strong in-plane anisotropic mechanical properties

In addition to out-of-plane NPR, in-plane NPR is a common phenomenon for 2-D crystals.⁴³⁻⁴⁶ For orthogonal symmetric 2-D crystals, their constitutive relation of linear elasticity can be represented as⁵⁷

$$\begin{bmatrix} \sigma_{xx} \\ \sigma_{yy} \\ \sigma_{xy} \end{bmatrix} = \begin{bmatrix} C_{11} & C_{12} & 0 \\ C_{12} & C_{22} & 0 \\ 0 & 0 & C_{66} \end{bmatrix} \begin{bmatrix} \varepsilon_{xx} \\ \varepsilon_{yy} \\ 2\varepsilon_{xy} \end{bmatrix} \quad (1)$$

To get the elastic coefficient C_{ij} , we calculate the strain energy of 2-D X_3M_2 $E_s(\varepsilon_{xx}, \varepsilon_{yy}, \varepsilon_{xy})$ in a $5 \times 5 \times 5$ grid of the $(\varepsilon_{xx}, \varepsilon_{yy}, \varepsilon_{xy})$ strain space within $\pm 1\%$, and then derive the elastic coefficient C_{11} , C_{22} , C_{12} and C_{66} through parabolic fitting of the strain potential energy surface with respect to ε_{xx} , ε_{yy} and ε_{xy} .⁵⁷ The calculated elastic constants for 2-D X_3M_2 (X=S, Se; M=N, P, As) are listed in Table 3. Besides, for elastic stability the elastic constants of orthorhombic systems should satisfy C_{11} , C_{22} , $C_{66} > 0$ and $C_{11}C_{22} > C_{12}^2$, which are undoubtedly satisfied by X_3M_2 studied in this work.⁵⁸

Table 3. Elastic constants for 2-D X_3M_2 (X=S, Se; M=N, P, As)

Formula	Stiffness constants (GPa)				Young's modulus (GPa)		Poisson's ratio		Shear modulus (GPa)
	C_{11}	C_{22}	C_{12}	C_{66}	E_{xx}	E_{yy}	ν_{xx}	ν_{yy}	G
S_3N_2	84.16	33.83	25.05	34.43	65.62	26.38	0.741	0.298	34.43

Se_3N_2	89.69	34.97	14.62	33.61	83.57	32.59	0.418	0.163	33.61
S_3P_2	76.23	20.97	17.26	20.11	62.03	17.07	0.823	0.226	20.11
Se_3P_2	67.05	13.22	15.27	19.11	49.40	9.74	1.155	0.228	19.11
S_3As_2	54.83	14.96	14.78	17.62	40.23	10.97	0.988	0.270	17.62
Se_3As_2	66.37	13.40	14.47	18.96	50.75	10.24	1.080	0.218	18.96

Then, the in-plane Young's modulus $E(\theta)$ and Poisson's ratio $\nu(\theta)$ in direction θ for orthogonal symmetric 2-D crystals are derived as⁵⁷,

$$\nu(\theta) = \frac{v_{ZZ}\cos^4\theta + v_{ZZ}\sin^4\theta - d_1\sin^2\theta\cos^2\theta}{\cos^4\theta + d_2\sin^2\theta\cos^2\theta + d_3\sin^4\theta} \quad (2)$$

$$E(\theta) = \frac{Y_{ZZ}}{\cos^4\theta + d_2\sin^2\theta\cos^2\theta + d_3\sin^4\theta} \quad (3)$$

where d_1 , d_2 , d_3 , Y_{ZZ} and v_{ZZ} are variables defined with elastic constants C_{ij} (see SI, Equation S1). The above relations have successfully described the orientation-dependent mechanical properties of orthogonal symmetric 2-D crystals, like black phosphorene and δ -P.^{45, 59}

Figure 5(a) shows the orientation-dependent in-plane Young's modulus $E(\theta)$ for α -heart structure S_3N_2 . The maximum Young's modulus is found to be 82.26 GPa at $\theta = 30^\circ$ (with respect to x axis), different from the intuition that extreme points always stay at the high symmetrical direction (i.e. x or y direction). Figure 5(b) shows the orientation dependent in-plane Poisson's ratio. Surprisingly, the in-plane NPR is observed around $\theta = 45^\circ$ (Considering the structural symmetry, $\theta = 45^\circ$ means two symmetric in-plane principal axes at $\theta_1 = 45^\circ$ and $\theta_2 = 180 - 45^\circ$, see Figure 5(c)) with a minimum value of -0.0259 at $\theta = 45^\circ$. It is the first time to find the 2-D crystal with both of the out-of-plane and in-plane NPR, an unusual 3-D auxetic property.

For β -heart structure S_3P_2 , we have found that the maximum Young's modulus is 63.60 GPa at $\theta = 17^\circ$, and the minimum value is 17.07 GPa at $\theta = 90^\circ$ (see Figure 5(d)). Besides, we have also found for all of the 2-D X_3M_2 ($\text{X}=\text{S}, \text{Se}$; $\text{M}=\text{N}, \text{P}, \text{As}$) the minimum Young's modulus is reached at $\theta = 90^\circ$, which means that y direction is always the softest direction for the 2-D crystals with heart-shaped structures. Figure 5(e) shows the orientation-dependent in-plane Poisson's ratio, and the minimum Poisson's ratio is 0.0157 at $\theta = 45^\circ$ instead of a negative value. Note that S_3P_2 is the only 2-D crystal that doesn't have NPR in in-plane

direction, and all of the other 2-D X_3M_2 ($X=S, Se; M=N, P, As$) except S_3P_2 show NPR in in-plane direction of certain angles (see SI, Figure S7 and Table S2). For example, Figure S15(d) shows $\nu(\theta)$ of Se_3As_2 has obvious in-plane NPR around $\theta = 42^\circ$ and a minimum value of -0.1857.

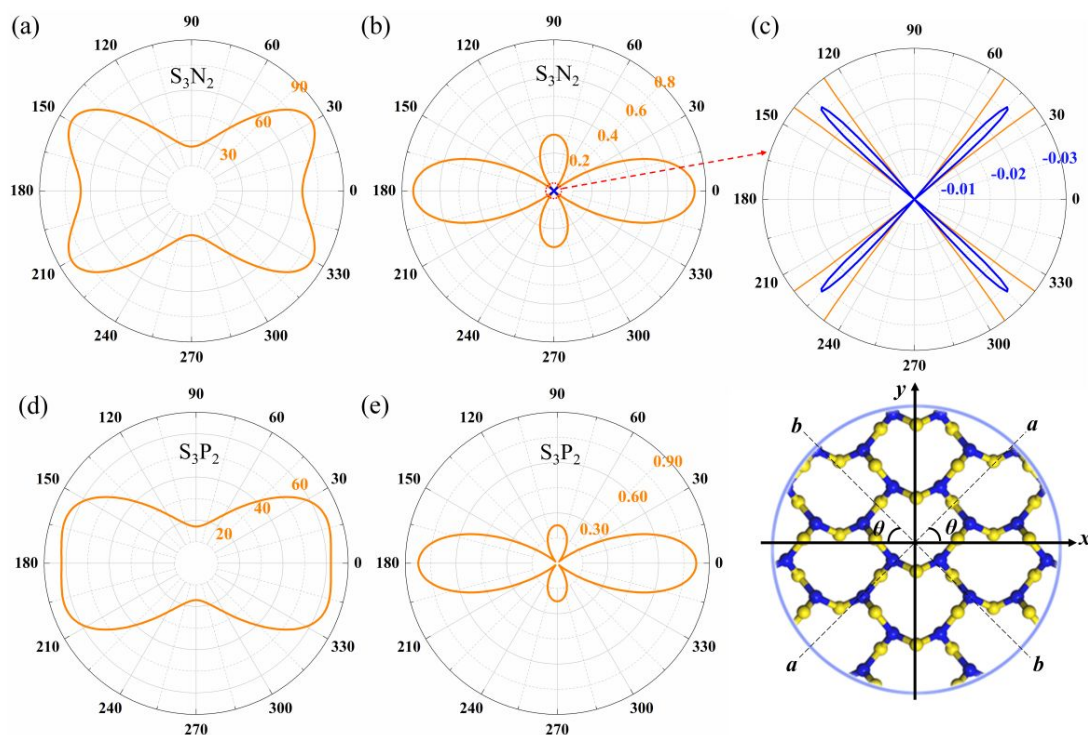


Figure 5. Orientation-dependent in-plane Young's modulus $E(\theta)$ (a) and Poisson's ratio $\nu(\theta)$ (b) for α -heart structure S_3N_2 . (c) Poisson's ratio in the red dash circle of (b). Two in-plane principal axes are shown as a - a and b - b . Young's modulus $E(\theta)$ (d) and Poisson's ratio $\nu(\theta)$ (e) of for β -heart structure S_3P_2 . Orange and blue colored curves indicate positive and negative Poisson's ratio, respectively. Here, the unit of Young's modulus is GPa.

Interestingly, the orientation-dependent in-plane Young's modulus and Poisson's ratio have almost the same shapes (see SI, Figure S15), even though the value and position of the extreme of Young's modulus and Poisson's ratio have somehow different (see SI, Table S2). Furthermore, the two types of topological structures, i.e. α -heart and β -heart, don't exhibit obvious effects on the orientation-dependent in-plane mechanical properties, that is, we attribute the distinctive in-plane mechanical behaviors of 2-D X_3M_2 to the novel heart-shaped structure. Instead, the α -heart and β -heart topological structures have a significant effect on out-

of-plane mechanical behaviors due to structural difference in out-of-plane direction.

4. Conclusions

In this work, the mechanical behaviors for a series of 2-D crystals X_3M_2 ($X=S, Se$; $M=N, P, As$) are explored through density functional theory (DFT) calculations. There are two atomic structures for 2-D X_3M_2 , namely α -heart and β -heart, exhibiting different mechanical and electrical properties. Energy band structures for α -heart and β -heart are direct and indirect, respectively, and the band gap decreases with increasing atomic number for the same structure. Different out-of-plane NPR phenomena are observed due to out-of-plane structural difference, that is, α -heart structure exhibits general out-of-plane NPR under in-plane tension in y direction, while β -heart structure exhibits general out-of-plane NPR under in-plane tension in x direction. Through DFT calculations, we revealed that NPR is a general phenomenon for 2-D X_3M_2 , and the absolute value of out-of-plane NPR for 2-D X_3M_2 is one order of magnitude larger than other reported 2-D crystals in general. At the same time, the in-plane NPR at certain angle around two in-plane principal axes also exists for 2-D X_3M_2 except S_3P_2 . Unusual 3-D auxetic properties in 2-D crystals will enormously enrich the researches on novel mechanical, electrical and chemical behaviors of 2-D crystals. Our works extend the family of 2-D crystals with NPR, and shed lights on designing novel negative Poisson's ratio materials.

Supporting Information

Additional details for atom structures, out-of-plane strain and their corresponding Poisson's ratio, orientation-dependent in-plane Young's modulus $E(\theta)$, Poisson's ratio $\nu(\theta)$ of other 2-D crystals X_3M_2 (i.e. N_2Se_3 , P_2Se_3 , As_2S_3 and Se_3As_2) and energy band structures of 2D X_3M_2 . Additional details for X_3M_2 bulk crystals. The tables summarize extremes of the in-plane Young's modulus and Poisson's ratio for 2-D crystals X_3M_2 and Cross-plane interlayer Poisson's ratio for X_3M_2 bulk crystals.

Conflicts of interest

There are no conflicts of interest to declare.

Acknowledgment

Y.L. acknowledges the support from the National Key Research and Development Program of China (No. 2016YFB0700300) and National Natural Science Foundation of China (No. 11572239). X.C. acknowledges the support from the National Natural Science Foundation of China (Nos. 11372241 and 11572238), ARPA-E (DE-AR0000396) and AFOSR (FA9550-12-1-0159).

References

1. K. S. Novoselov, A. K. Geim, S. V. Morozov, D. Jiang, Y. Zhang, S. V. Dubonos, I. V. Grigorieva and A. A. Firsov, *Science*, 2004, **306**, 666-669.
2. X. Kong, Q. Liu, C. Zhang, Z. Peng and Q. Chen, *Chem Soc Rev*, 2017, **46**, 2127-2157.
3. M. Pumera and Z. Sofer, *Adv Mater*, 2017, **29**, 1605299.
4. A. J. Mannix, B. Kiraly, M. C. Hersam and N. P. Guisinger, *Nature Reviews Chemistry*, 2017, **1**.
5. B. Anasori, M. R. Lukatskaya and Y. Gogotsi, *Nature Reviews Materials*, 2017, **2**, 16098.
6. K. Kang, S. Xie, L. Huang, Y. Han, P. Y. Huang, K. F. Mak, C. J. Kim, D. Muller and J. Park, *Nature*, 2015, **520**, 656-660.
7. S. Zhang, M. Xie, F. Li, Z. Yan, Y. Li, E. Kan, W. Liu, Z. Chen and H. Zeng, *Angew Chem Int Ed Engl*, 2016, **55**, 1666-1669.
8. J. Zhou, J. Lin, X. Huang, Y. Zhou, Y. Chen, J. Xia, H. Wang, Y. Xie, H. Yu, J. Lei, D. Wu, F. Liu, Q. Fu, Q. Zeng, C. H. Hsu, C. Yang, L. Lu, T. Yu, Z. Shen, H. Lin, B. I. Yakobson, Q. Liu, K. Suenaga, G. Liu and Z. Liu, *Nature*, 2018, **556**, 355-359.
9. A. J. Mannix, X. F. Zhou, B. Kiraly, J. D. Wood, D. Alducin, B. D. Myers, X. Liu, B. L. Fisher, U. Santiago, J. R. Guest, M. J. Yacaman, A. Ponce, A. R. Oganov, M. C. Hersam and N. P. Guisinger, *Science*, 2015, **350**, 1513-1516.
10. J. Lang, B. Ding, S. Zhang, H. Su, B. Ge, L. Qi, H. Gao, X. Li, Q. Li and H. Wu, *Adv Mater*, 2017, **29**, 1701777.
11. M. E. Dávila, L. Xian, S. Cahangirov, A. Rubio and G. L. Lay, *New Journal of Physics*, 2014, **16**, 3579-3587.
12. F. F. Zhu, W. J. Chen, Y. Xu, C. L. Gao, D. D. Guan, C. H. Liu, D. Qian, S. C. Zhang and J. F. Jia, *Nature Materials*, 2015, **14**, 1020+.
13. P. Vogt, P. De Padova, C. Quaresima, J. Avila, E. Frantzeskakis, M. C. Asensio, A. Resta, B. Ealet and G. Le Lay, *Phys Rev Lett*, 2012, **108**, 155501.
14. S. Zhang, Z. Yan, Y. Li, Z. Chen and H. Zeng, *Angew Chem Int Ed Engl*, 2015, **54**, 3112-3115.
15. F. Reis, G. Li, L. Dudy, M. Bauernfeind, S. Glass, W. Hanke, R. Thomale, J. Schafer and R. Claessen, *Science*, 2017, **357**, 287-290.
16. L. Li, Y. Yu, G. J. Ye, Q. Ge, X. Ou, H. Wu, D. Feng, X. H. Chen and Y. Zhang, *Nat Nanotechnol*, 2014, **9**, 372-377.
17. H. Sahin, S. Cahangirov, M. Topsakal, E. Bekaroglu, E. Akturk, R. T. Senger and S. Ciraci, *Phys Rev B*, 2009, **80**, 155453.

18. J. N. Coleman, M. Lotya, A. O'Neill, S. D. Bergin, P. J. King, U. Khan, K. Young, A. Gaucher, S. De, R. J. Smith, I. V. Shvets, S. K. Arora, G. Stanton, H. Y. Kim, K. Lee, G. T. Kim, G. S. Duesberg, T. Hallam, J. J. Boland, J. J. Wang, J. F. Donegan, J. C. Grunlan, G. Moriarty, A. Shmeliiov, R. J. Nicholls, J. M. Perkins, E. M. Grieverson, K. Theuwissen, D. W. McComb, P. D. Nellist and V. Nicolosi, *Science*, 2011, **331**, 568-571.
19. M. Naguib, V. N. Mochalin, M. W. Barsoum and Y. Gogotsi, *Adv Mater*, 2014, **26**, 992-1005.
20. Q. H. Wang, K. Kalantar-Zadeh, A. Kis, J. N. Coleman and M. S. Strano, *Nat Nanotechnol*, 2012, **7**, 699-712.
21. R. Lakes, *Science*, 1987, **235**, 1038-1040.
22. R. H. Baughman, J. M. Shacklette, A. A. Zakhidov and S. Stafstrom, *Nature*, 1998, **392**, 362-365.
23. J. N. Grima, R. Jackson, A. Alderson and K. E. Evans, *Advanced Materials*, 2000, **12**, 1912-1918.
24. U. D. Larsen, O. Signund and S. Bouwsta, *Journal of Microelectromechanical Systems*, 1996, **6**, 99-106.
25. A. U. Ortiz, A. Boutin, A. H. Fuchs and F. X. Coudert, *Physical Review Letters*, 2012, **109**, 195502.
26. S. Banaee, J. Shim, J. C. Weaver, E. R. Chen, N. Patel and K. Bertoldi, *Adv Mater*, 2013, **25**, 5044-5049.
27. J. L. Silverberg, A. A. Evans, L. Mcleod, R. C. Hayward, T. Hull, C. D. Santangelo and I. Cohen, *Science*, 2014, **345**, 647.
28. Y. Suzuki, G. Cardone, D. Restrepo, P. D. Zavattieri, T. S. Baker and F. A. Tezcan, *Nature*, 2016, **533**, 369-373.
29. D. Prall and R. S. Lakes, *International Journal of Mechanical Sciences*, 1997, **39**, 305-307.
30. A. Alderson and K. L. Alderson, *P I Mech Eng G-J Aer*, 2007, **221**, 565-575.
31. J. B. Choi and R. S. Lakes, *International Journal of Fracture*, 1996, **80**, 73-83.
32. R. S. Lakes and K. Elms, *Journal of Composite Materials*, 1992, **27**, 1193-1202.
33. W. Yang, Z. M. Li, W. Shi, B. H. Xie and M. B. Yang, *Journal of Materials Science*, 2004, **39**, 3269-3279.
34. G. N. Greaves, A. L. Greer, R. S. Lakes and T. Rouxel, *Nat Mater*, 2011, **10**, 823-837.
35. Z. Y. Wang and H. Hu, *Textile Research Journal*, 2014, **84**, 1600-1611.
36. F. Scarpa, *IEEE Signal Processing Magazine*, 2008, **25**, 128-126.
37. J. W. Jiang and H. S. Park, *Nat Commun*, 2014, **5**, 4727.
38. H. Wang, X. Li, J. Sun, Z. Liu and J. Yang, *2D Materials*, 2017, **4**, 045020.
39. J. Han, J. Xie, Z. Zhang, D. Yang, M. Si and D. Xue, *Applied Physics Express*, 2015, **8**, 041801.
40. L. C. Zhang, G. Qin, W. Z. Fang, H. J. Cui, Q. R. Zheng, Q. B. Yan and G. Su, *Sci Rep*, 2016, **6**, 19830.
41. Y. Du, J. Maassen, W. Wu, Z. Luo, X. Xu and P. D. Ye, *Nano Letters*, 2016, **16**, 6701-6708.
42. L. Kou, Y. Ma, C. Tang, Z. Sun, A. Du and C. Chen, *Nano Lett*, 2016, **16**, 7910-7914.
43. S. Zhang, J. Zhou, Q. Wang, X. Chen, Y. Kawazoe and P. Jena, *Proceedings of the National Academy of Sciences*, 2015, **112**, 2372.
44. Y. Wang, F. Li, Y. Li and Z. Chen, *Nat Commun*, 2016, **7**, 11488.
45. H. Wang, X. Li, P. Li and J. Yang, *Nanoscale*, 2016, **9**, 850.
46. X. Liu, X. Shao, B. Yang and M. Zhao, *Nanoscale*, 2018, **10**, 2108-2114.

47. H. Xiao, X. Shi, X. Liao, Y. Zhang and X. Chen, *Phys Rev Mater*, 2018, **2**, 024002.
48. H. Xiao, X. Shi, Y. Zhang, M. Li, X. Liao and X. Chen, *Computational Materials Science*, 2018, **155**, 288-292.
49. N. Morimoto, *Journal of Mineralogical & Petrological Sciences*, 1956, **1**, 160-169.
50. A. L. Renninger and B. L. Averbach, *Acta Crystallographica*, 1973, **29**, 1583-1589.
51. P. Giannozzi, S. Baroni, N. Bonini, M. Calandra, R. Car, C. Cavazzoni, D. Ceresoli, G. L. Chiarotti, M. Cococcioni, I. Dabo, A. Dal Corso, S. de Gironcoli, S. Fabris, G. Fratesi, R. Gebauer, U. Gerstmann, C. Gougoussis, A. Kokalj, M. Lazzeri, L. Martin-Samos, N. Marzari, F. Mauri, R. Mazzarello, S. Paolini, A. Pasquarello, L. Paulatto, C. Sbraccia, S. Scandolo, G. Sclauzero, A. P. Seitsonen, A. Smogunov, P. Umari and R. M. Wentzcovitch, *J Phys Condens Matter*, 2009, **21**, 395502.
52. P. JP, B. K and E. M, *Physical Review Letters*, 1996, **77**, 3865.
53. H. J. Monkhorst and J. D. Pack, *Phys Rev B*, 1976, **13**, 5188.
54. S. Grimme, *J Comput Chem*, 2006, **27**, 1787-1799.
55. L. J. Sham and M. Schluter, *Physical Review Letters*, 1983, **51**, 1888-1891.
56. J. P. Perdew and M. Levy, *Physical Review Letters*, 1983, **51**, 1884-1887.
57. Q. Wei and X. H. Peng, *Appl Phys Lett*, 2014, **104**, 372-398.
58. F. Mouhat and F.-X. Coudert, *Phys Rev B*, 2014, **90**, 224104.
59. L. Wang, A. Kutana, X. Zou and B. I. Yakobson, *Nanoscale*, 2015, **7**, 9746-9751.